Fast and Flexible Selective Harmonic Extraction Methods Based on the Generalized Discrete Fourier Transform

Huawu Liu, *Student Member, IEEE*, Haibing Hu, *Member, IEEE*, Hao Chen, Li Zhang, *Member, IEEE*, and Yan Xing, *Member, IEEE*

***Abstract*—Selective harmonic extraction plays an important role in power quality assessment, harmonic compensation, and so on. Among the various methods, discrete Fourier transform (DFT)-based algorithms has found wide and popular applications due to advantages like simplicity and excellent selectively filtering properties. However, DFT suffers from disadvantages like slow dynamics and sensitivity to frequency variations. In order to alleviate these drawbacks, an improved and extended DFT—generalized DFT (GDFT) is proposed. It is revealed in this paper that the conventional DFT can be viewed as a comb filter connected in series with complex resonators, and DFT relies on the mechanism of *pole-zero cancellation* for harmonic extraction. More importantly, the key reason behind the DFT slow transient responses is the large delay introduced by the comb filter. Therefore, this paper proposed to reconfigure the comb filter according to specific harmonic patterns of the input signal for improving the dynamic responses and system flexibility. The proposed GDFT not only maintains the advantages of simplicity and selectively filtering properties but also features fast transients, around 0.3 fundamental cycle for typical applications, which is much shorter than the one-cycle settling time of the conventional DFT. A phase-locked-loop block is also incorporated into the harmonic-detection system to deal with possibly large frequency variations in practical applications. Extensive tests are provided to validate effectiveness of the proposed method.**

***Index Terms*—Fourier transform, harmonic detection, phase-locked-loop, three phase.**

I. Introduction

SELECTIVE harmonic-extraction has found wide applications in many occasions [1]–[6]. In the harmonic compensation devices, harmonic extraction is the key part [1]–[4]. The active power filter (APF), which has a long history of practical use for compensating the harmonic currents generated by nonlinear loads, is a very typical example. Distorted load currents need to be first detected before feeding to the current controller as references for tracking. Issues of accuracy, dynamic performances, and implementation complexity, etc., shall be taken into consideration in detection technique design. Another typical application is grid-synchronization under adverse conditions [5], [6], which are often required by grid-connected converters, like rectifiers for motor drive systems and chargers for electric vehicles. For these applications, the fundamental voltage component usually needs to be first isolated from harmonic-polluted grid signals before entering the phase/frequency-locked loops, and performances of the harmonic detection determines both the synchronization accuracy and its dynamics [7].

Various harmonic methods have been researched in the literatures [7]–[25], which can be generally categorized into time-domain and frequency-domain methods [1], [7]. Typical time-domain methods include, second-order generalized integrators (SOGI) methods [8], fundamental/harmonic-*dq*-frame methods [1], [9], multiple-reference-frame (MRF) methods [10], [11], adaptive notch filter (ANF) approaches [12], [13] the cascaded-delayed-signal-cancellation (CDSC) techniques [7], [14], the instantaneous power theory (*pq* power theory) methods [15], the advanced Kalman-filter methods [16] etc. While these time-domain methods can effectively extract the harmonic components, there exist some limitations. The SOGI and the *dq*-frame -based methods need to make a tradeoff between steady state accuracy and dynamics [1]. The MRF-based, the ANF-based, and the Kalman-filter-based approaches are essentially based on the concept of harmonic decoupling [17]. Good accuracy and relatively fast dynamics can be achieved. However, they are lack of selectivity—all the harmonic components with non-negligible magnitudes must be estimated and extracted at the same time even though some of them are not desired. The *pq*-theory techniques only estimate the fundamental signal and detect the rest harmonics as a whole, and are therefore incapable of selective harmonic extraction. The CDSC-based methods can achieve relatively shorter transients with good accuracy. They are based on constructing a series of DSC operators, which consists of high-order delay buffers to separate the desired component and filter out the rest; therefore, for extracting each harmonic, different sets of DSC operators are required, which can

Manuscript received September 13, 2016; revised December 1, 2016 and February 7, 2017; accepted April 26, 2017. Date of publication May 10, 2017; date of current version January 3, 2018. This work was supported in part by the National Natural Science Foundation of China under Grant 5157708 and Grant 51677054, and in part by Joint Research of Industry and Academia of Jiangsu Province under Grant 2015003-008. Recommended for publication by Associate Editor Friedrich W. Fuchs. *(Corresponding Author: Yan Xing.)*

H. Liu, H. Hu, H. Chen, and Y. Xing are with the College of Automation, Nanjing University of Aeronautics and Astronautics, Nanjing 210016, China (e-mail: liuhuawu@nuaa.edu.cn; huhaibing@nuaa.edu.cn; chenhao@nuaa.edu.cn; xingyan@nuaa.edu.cn).

L. Zhang is with the College of Energy and Electrical Engineering, Hohai University, Nanjing 211100, China (e-mail: zhanglinuaa@hhu.edu.cn).

Color versions of one or more of the figures in this paper are available online at http://ieeexplore.ieee.org.

Digital Object Identifier 10.1109/TPEL.2017.2703138

increase the system complexity, computational effort, and storage memory overhead especially when many harmonic components are to be extracted in applications like the selective APF.

Frequency-domain methods typically refer to the Fourier transform based techniques [18]–[25]. Discrete Fourier transform (DFT) methods mathematically transform discrete signals to the frequency domain with prominent features like simplicity, enhanced selectivity and steady state accuracy. The fast Fourier transform implements the DFT in a different form to reduce the computational burden and is widely used for harmonic monitoring and metering [1]. To further reduce the calculation burden for real-time applications, the sliding recursive DFT (SDFT) has gained wide interests in recent years [20]–[24]. The SDFT essentially calculates a DFT on a sample-by-sample basis with the window shifting every sampling instant for a fixed number of samples, usually just one for simplicity. Jacobsen and Lyons [22], demonstrate the mathematical derivation of SDFT from the DFT and Goertzel algorithm. Although the SDFT is computational efficient, it may suffer from accumulated errors and potentially instability. Therefore, Duda [24] proposed an improved, guaranteed stable algorithm based on the DFT modulation property. The SDFT has found wide applications. In [20] and [21], the SDFT was utilized for grid-synchronization and extraction of harmonic voltage components. In [25], the SDFT was applied for current control to suppress specific harmonics. The major drawback of the above Fourier-based harmonic detection methods, as evaluated in [1], [7], is the slow dynamic responses, requiring at least one-cycle settling time. Besides, careful synchronization between the sampling and fundamental frequency is needed in practical applications to minimize leakage effects of DFT, and in case of large frequency deviation, significant errors both in magnitude and phase angle can be introduced.

To alleviate the aforementioned drawbacks of slow dynamics and sensitivity to frequency variation, an improved and generalized DFT (GDFT) is proposed. The key idea is to reconfigure and reconstruct the conventional DFT according to the specific harmonic scenario of the input signal for improving system dynamics and flexibility. The transfer function perspective is adopted in Section II to analyze the filtering mechanism and key reasons behind the slow dynamics of DFT. And, in order to improve the dynamics, the proposed solution is presented in Section III. Considerations of discrete implementation and frequency adaptability of the GDFT are given in Section IV. Extensive tests are shown in Section V. Section VI concludes this paper.

II. Transfer Function Interpretation of the DFT

A. Description of DFT

DFT mathematically transforms the input discrete signals into frequency-domain [20]

$$\hat{X}^k_{\alpha\beta}(n) = \sum_{i=n-N+1}^{n} \left[\vec{x}_{\alpha\beta}(i) e^{-j2\pi \frac{i}{N}k}\right], \quad k = 0, \pm 1, \ldots, \pm\left(\frac{N}{2} - 1\right) \tag{1}$$

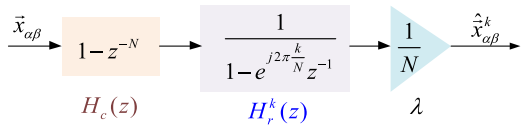

Fig. 1. Block diagram of DFT.

where $\vec{x}_{\alpha\beta}(i)$ is the input vector signal obtained through sampling the time-domain signal $\vec{x}_{\alpha\beta}(t)$ with a rate of $f_s = N\omega_0/2\pi$;$\hat{X}^k_{\alpha\beta}(n)$ refers to the DFT's kth-bin frequency component, and n is a time-sequence index. And the time-domain expression for the sequence of the kth harmonic at the current time-sequence (i.e., n) can be obtained through the inverse DFT

$$\hat{\vec{x}}^k_{\alpha\beta}(n) = \frac{1}{N}\hat{X}^k_{\alpha\beta}(n) e^{j2\pi\frac{kn}{N}}. \tag{2}$$

Equations (1) and (2) are the key equations for harmonic extraction based on the DFT. However, direct calculations of the DFT based on (1) and (2) are highly computational demanding. Thus in recent years, the SDFT has been proposed to reduce the computational burden [24],

$$\hat{X}^k_{\alpha\beta}(n) = \hat{X}^k_{\alpha\beta}(n-1) + \left[\vec{x}_{\alpha\beta}(n) - \vec{x}_{\alpha\beta}(n-N)\right] e^{-j2\pi\frac{k}{N}(n-1)} \tag{3}$$

where $\hat{X}^k_{\alpha\beta}(n)$ is the spectral vector for the current window of the sequence $\{\vec{x}_{\alpha\beta}(i),\ i = n-N+1,\ n-N,\ n-N-1, \ldots, n\}$; and $\hat{X}^k_{\alpha\beta}(n-1)$ is the spectral vector for the previous window of $\{\vec{x}_{\alpha\beta}(i),\ i = n-N,\ n-N+1, \ldots, n-1\}$.

B. Transfer Function Interpretation of DFT

Analysis of the DFT based on (1)–(3) is difficult and inconvenient. Therefore, the z-transform is applied and mathematical manipulations (see Appendix A for details) are performed to derive its transfer function

$$G^k_{\mathrm{DFT}}(z) = \frac{Z\left[\hat{\vec{x}}^k_{\alpha\beta}(n)\right]}{Z\left[\vec{x}_{\alpha\beta}(n)\right]} = \frac{1}{N}\frac{1-z^{-N}}{1-e^{j2\pi\frac{k}{N}}z^{-1}} = \underbrace{\left(1-z^{-N}\right)}_{H_c(z)} \underbrace{\frac{1}{1-e^{j2\pi\frac{k}{N}}z^{-1}}}_{H_r^k(z)} \underbrace{\frac{1}{N}}_{\lambda} \tag{4}$$

where $G^k_{\mathrm{DFT}}(z)$ refers to the transfer function from the extracted kth harmonic $\hat{\vec{x}}^k_{\alpha\beta}(n)$ to the input signal $\vec{x}_{\alpha\beta}(n)$. To better analyze the properties of DFT, $G^k_{\mathrm{DFT}}(z)$ in (4) can be divided into three parts, $H_c(z)$, $H_r^k(z)$ and λ, as shown in Fig. 1.

$H_c(z)$ is a typical finite-impulse-response filter, and is often referred to as the comb filter in the field of digital signal processing, with the most distinguishing characteristic being that it has multiple equiripple lobes in the frequency response as clearly shown by the bode plot in Fig. 2.

The comb filter $H_c(z)$ can be further expanded as

$$H_c(z) = 1 - z^{-N} = \prod_{n=0}^{N-1}\left(1 - e^{j\frac{2\pi}{N}n}z^{-1}\right). \tag{5}$$

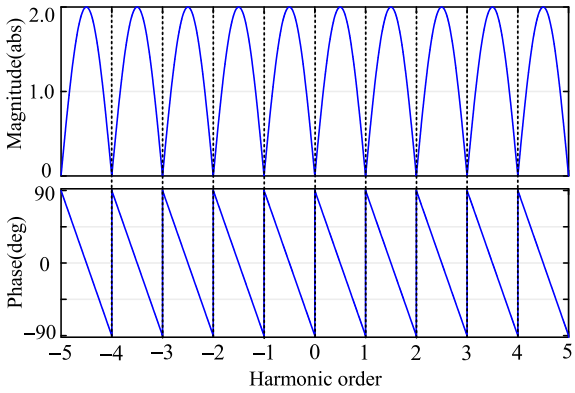

Fig. 2. Frequency response of the comb filter $H_1(z)$, $N = 32$, $\omega_0 = 100\,\pi$.

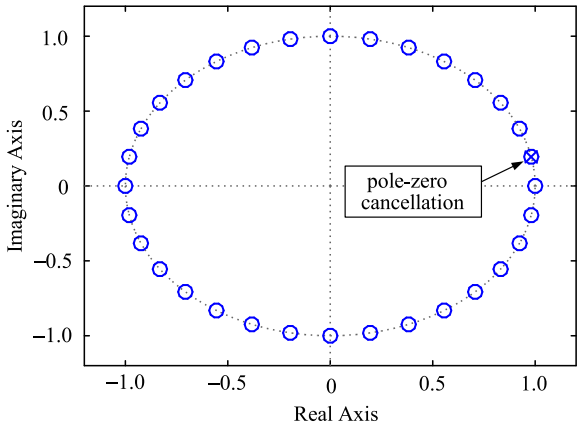

Fig. 3. Pole-zero diagram of the DFT filter $G^k_{\mathrm{DFT}}(z)$, $N = 32$, $k = 1$.

Equation (5) implies an important property—N zeros are introduced, which are centered at integer multiples of the fundamental frequency $\omega = k\omega_0$ ($\omega_0 = 2\pi/N, k = 0, 1, \ldots, N-1$) and are evenly distributed on the unit circle. The introduced zeros guarantee that complete rejections of the harmonics at the corresponding frequencies are achieved, if the fundamental period of the applied signal equal to the time window NT_{s}. This property can be better visualized by the notches, i.e., zero amplitude, in the frequency response of the comb filter in Fig. 2.

The filter $H^k_r(z)$ is essentially a complex resonator, helping to isolate and extract the desired kth harmonic. It can be seen from (4) that $H^k_r(z)$ produces a pole $p = \exp(j2\pi k/N)$ on the z-domain unit circle, meaning that a ***pole-zero cancellation*** at the kth-harmonic frequency is obtained as shown in Fig. 3. And, implications of the pole-zero cancellation are as follows.

1) Rejection of kth harmonic due to the zero introduced by the comb filter $H_{\mathrm{c}}(z)$ is now offset by the pole provided by $H^k_r(z)$, and its spectrum information is reserved and isolated. Therefore, extraction of the desired kth harmonic from other harmonic components are now achieved.
2) The DFT filter has a finite impulse response and is unconditionally stable [20].

Finally, the gain λ in Fig. 1 helps to adjust the amplitude of the selected kth harmonic. To further analyze the filtering abilities of the conventional DFT, frequency responses of $G^k_{DFT}(z)$ are plotted in Fig. 4. As expected, at the selected frequency ($f = 50$ Hz), zero attenuation and phase-shift are achieved, while at other harmonic frequencies, total rejection (zero magnitude) is achieved. Moreover, the DFT exhibits band-passing properties with magnitude envelop asymptotes of $+20$ and -20 dB/dec at low and high frequencies. These characteristics further enhance filtering abilities by helping to attenuate the subharmonics of the input signal.

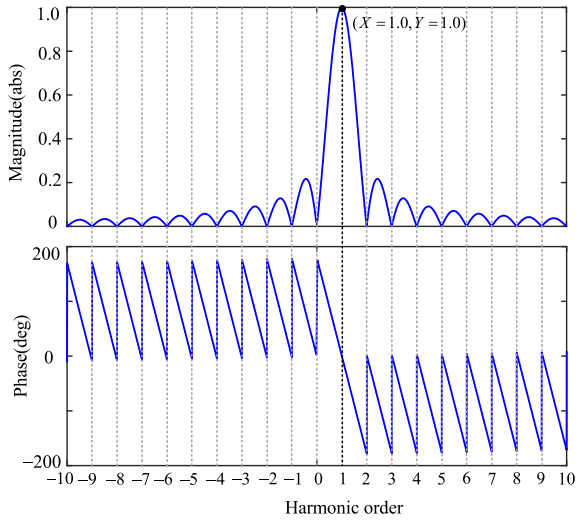

Fig. 4. Frequency response of the DFT filter $G^k_{\mathrm{DFT}}(z)$, $N = 198$, $k = 1$, $\omega_0 = 100\,\pi$.

C. Filtering Mechanism of DFT and Its Major Drawback

According to the above analysis, it can be concluded that DFT "takes three steps" to isolate and extract a specific harmonic from the applied input signal:

Step I: A set of ***zeros***, located at the integer-harmonic frequencies $\omega = k\omega_0$ ($k = 0, 1, \ldots, N-1$), are introduced by the comb filter $H_{\mathrm{c}}(z)$ to achieve complete rejection of the harmonics (see (5) and Fig. 2).

Step II: The complex resonator $H^k_r(z)$ is utilized to produce a ***pole*** at the selected frequency to achieve ***pole-zero cancellation*** and to isolate and extract the desired harmonic component (see Figs. 3 and 4).

Step III: Magnitude of the selected harmonic is performed by the gain λ.

In short, the key mechanism behind the DFT filter is the "***pole-zero cancellation***". And, in the process, the comb filter plays a crucial role.

1) The comb filter determines the introduced zeros and the set of harmonics to be rejected. In the conventional DFT, the comb filter $H_{\mathrm{c}}(z)$ introduces N-zeros equidistantly located at the z-domain unit circle to reject all the harmonic components of integer multiples of the fundamental frequency. However, some of the zeros may be unnecessary and redundant. For example, consider that even harmonics are seldom found in practical applications (or their amplitudes are much smaller and can be neglected). And, in a three-phase power systems, the typical harmonic

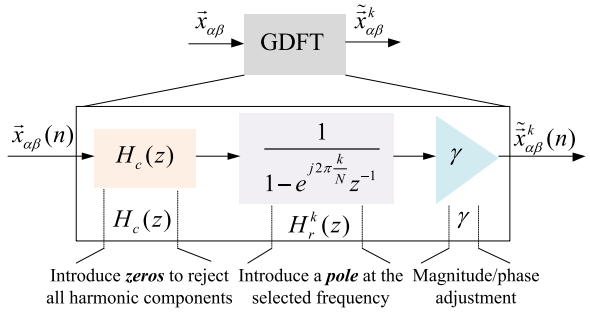

Fig. 5. Structure diagram of the proposed GDFT filter.

scenario is the nontriple odd harmonics $h = +1, -1, -5, +7, +13, -17$ or $h = \pm1, \pm5, \pm7, \pm13, \pm17, \ldots$, for heavily distorted conditions [11], [26]. In short, the conventional DFT cannot be configured for applications with specific harmonic scenarios, and the redundant zeros can result in unnecessary time-delay during dynamics.

2) The comb filter determines the DFT transient response. The comb filter consists of N delay-buffers in order to introduce N zeros; and in practical applications, the DFT algorithm is often initialized with zero input and zero output. Thus, the DFT output will not reach the steady state until N input samples have been processed, requiring at least one fundamental cycle for transient responses [22].

III. Proposed GDFT

In the previous section, it is shown that the major drawback of the conventional DFT lies in the comb filter, which hinders fast and flexible harmonic extraction. Concerning this problem, an extended and generalized version of DFT—GDFT is proposed in Fig. 5, where the comb filter $H_c(z)$ and the gain γ are entirely reconfigured and reconstructed into more general structures.

A. Configurations and Design of the GDFT

The proposed GDFT shown in Fig. 5 consists of three major parts, i.e., the comb filter $H_c(z)$, the complex resonator $H_r^k(z)$, and the magnitude/phase adjustment factor γ.

1) The comb filter $H_c(z)$

The aim of the $H_c(z)$ is to introduce a set of zeros for complete rejection of the harmonic components present in the applied input signal $\vec{x}_{\alpha\beta}$. Consider a general periodic signal with a harmonic scenario of $h = mk+l$, where m, l are integers, and $m>0$, $k = 0, \pm1, \ldots$. Substituting $z = z^{1/m}e^{-j2\pi l/mN}$ into (5), it yields

$$\begin{aligned} H_c(z) &= 1 - z^{-\frac{N}{m}}e^{j\frac{2\pi l}{m}} \\ &= \left(1 - e^{j\frac{2\pi}{Nm}l}z^{-\frac{1}{m}}\right)\left(1 - e^{j\frac{2\pi}{Nm}(m+l)}z^{-\frac{1}{m}}\right) \\ &\quad \cdots \left(1 - e^{j\frac{2\pi}{Nm}[(N-1)m+l]}z^{-\frac{1}{m}}\right) \\ &= \prod_{k=0}^{N-1}\left(1 - e^{j\frac{2\pi}{Nm}(mk+l)}z^{-\frac{1}{m}}\right). \end{aligned} \tag{6}$$

Setting $H_c(z) = 0$, the introduced zeros can easily be obtained as $\omega = (mk + l)\omega_0$ $(k = 0, 1, 2, \ldots, N-1)$. Comparing (6) of the proposed GDFT and (5) of the conventional DFT, it can be clearly seen that the delay samples of $H_c(z)$ are reduced to N/m, implying that the delay time of the GDFT is shortened to $1/m$ fundamental cycle.

To more clearly see the rejection properties of the comb filter $H_c(z)$ due to the introduced zeros, consider a input sequence $\vec{x}_{\alpha\beta}(n) = \sum_k V_k e^{j\omega_0(mk+l)n+\varphi_k}$ with harmonic orders of $h = mk+l$, where V_k and φ_k are the magnitude and phase angle;ω_0 the fundamental frequency. Applying the signal to the comb filter $H_c(z)$ in (6) to $\vec{x}_{\alpha\beta}(n)$, the steady state filtered output can be obtained as

$$\begin{aligned} \vec{y}_{\alpha\beta}(n) &= \vec{x}_{\alpha\beta}(n) - e^{j\frac{2\pi l}{m}}\vec{x}_{\alpha\beta}\left(n - \frac{N}{m}\right) \\ &= \sum_k V_k e^{j\omega_0(mk+l)n+\varphi_k} \\ &\quad - e^{j\frac{2\pi l}{m}}\sum_k V_k e^{j\omega_0(mk+l)\left(n-\frac{N}{m}\right)+\varphi_k} = 0. \end{aligned} \tag{7}$$

It can be observed from (7) that the harmonics with frequency orders of $h = mk+l$ are completely blocked.

The filter in (6) can only reject one set of harmonics. For applications with complicated harmonic scenarios, multiple ones of the comb filter can be connected in series

$$\begin{aligned} H_c(z) = &\left(1 - z^{-\frac{N}{m_1}}e^{j\frac{2\pi l_1}{m_1}}\right)\left(1 - z^{-\frac{N}{m_2}}e^{j\frac{2\pi l_2}{m_2}}\right) \\ &\cdots\left(1 - z^{-\frac{N}{m_p}}e^{j\frac{2\pi l_p}{m_p}}\right) \end{aligned} \tag{8}$$

where m_1–m_p, l_1–l_p are integers and m_1–$m_p>0$. Applying the comb filter of (8), harmonic components with orders of $h_1 = m_1k+l_1$, $h_2 = m_2k+l_2$, $\ldots$, $h_p = m_pk+l_p$, can be completely rejected.

2) The complex resonator $H_r^k(z)$

The complex resonator is the same as that of the conventional DFT in Fig. 1; it is required to isolate and extract the selected component through pole-zero cancellation.

3) The magnitude/phase adjustment factor γ

The aim of γ is to properly adjust the gain and phase of the extracted output signal. In the conventional DFT, γ is simply set to $1/N$. However, in the proposed GDFT, it is more complicated due to the flexible structure of the comb filter $H_c(z)$.

From Fig. 5, the transfer function of the proposed GDFT is

$$H_{\mathrm{GDFT}}^k(z) = \gamma H_c(z)H_r^k(z) = \frac{\gamma H_c(z)}{1 - e^{j2\pi\frac{k}{N}}z^{-1}}. \tag{9}$$

The aim is to ensure zero attenuation and zero phase-shift at the selected (kth-harmonic) frequency,

$$H_{\mathrm{GDFT}}^k(z)\big|_{z=e^{j2\pi\frac{k}{N}}} = \gamma H_c(z)H_r^k(z)\Big|_{z=e^{j2\pi\frac{k}{N}}} = 1. \tag{10}$$

Direct calculation of γ according to (10) is impossible since the numerator and the denominator at the selected frequency $z = e^{j2\pi\frac{k}{N}}$ both equals to 0, i.e.,$\gamma H_c(z)\big|_{z=e^{j2\pi\frac{k}{N}}} = 0$, $(1 - e^{j2\pi\frac{k}{N}}z^{-1})\big|_{z=e^{j2\pi\frac{k}{N}}} = 0$. Yet, the ***L'Hôspital's Rule for***

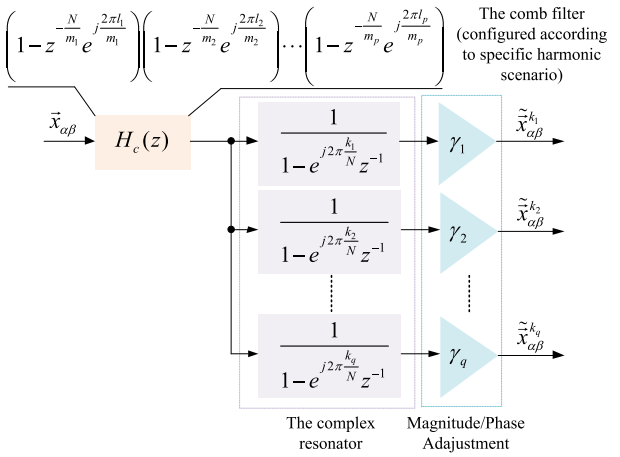

Fig. 6. Structure diagram of the proposed GDFT filter for extracting multiple harmonic components.

complex-value Functions can be utilized to derive the value of γ [27]

$$H^k_{GDFT}(z)\Big|_{z=e^{j2\pi\frac{k}{N}}} = \lim_{z\to z=e^{j2\pi\frac{k}{N}}} \frac{[\gamma H_c(z)]'}{\left(1-e^{j2\pi\frac{k}{N}}z^{-1}\right)'} = \frac{\gamma[H_c(z)]'}{e^{j2\pi\frac{k}{N}}z^{-2}}\Big|_{z=e^{j2\pi\frac{k}{N}}} = \frac{\gamma[H_c(z)]'\Big|_{z=e^{j2\pi\frac{k}{N}}}}{e^{-j2\pi\frac{k}{N}}}. \quad (11)$$

Combing (10) and (11) yields

$$\gamma = \frac{e^{-j2\pi\frac{k}{N}}}{[H_c(z)]'\Big|_{z=e^{j2\pi\frac{k}{N}}}} \quad (12)$$

where $[H_c(z)]'$ is the differential function of $H_c(z)$.

Moreover, Fig. 5 illustrates the diagram of extracting only one harmonic component. In case multiple components are desired, the complex resonators $H_r(z)$ and gain operations γ can be paralleled while the comb filter $H_c(z)$ is shared as shown in Fig. 6.

B. Features and Advantages of the Proposed GDFT

1) The GDFT is essentially a generalized version of the conventional DFT. In the conventional DFT, the comb filter introduces N ***zeros***, located at the harmonic frequencies of $\omega = k\omega_0$ ($\omega_0 = 2\pi/N, k = 0, 1, \ldots, N-1$), for isolating desired harmonic components and rejecting of the rest harmonics. However, some of the ***zeros*** are unnecessary since in practical applications, the input signal usually contains specific harmonic orders. For example, the non-triplen odd harmonics of order $+1$, -1, -5, $+7$, $+13$, and -17 are more often found in three-phase grid systems [26]. The proposed GDFT, which can be flexibly configured for specific harmonic scenarios through setting the desired ***zeros*** based on (8), is more suitable.

TABLE I
PARAMETERS OF THE PROPOSED GDFT: AN EXAMPLE

Items	Parameters
Harmonic pattern	$h = \pm1, \pm5, \pm7, \pm13, \pm17, \ldots$
Transfer function	$H^k_{\text{GDFT}} = \gamma H_c(z) H^k_r(z)$
The comb filter $H_c(z)$	$\left(1 - z^{-\frac{N}{6}} e^{j\frac{2\pi}{6}}\right)\left(1 - z^{-\frac{N}{6}} e^{-j\frac{2\pi}{6}}\right)$
Total delay time	$1/6 + 1/6 = 1/3$ fundamental cycle
The digital resonator $H^k_r(z)$	$\frac{1}{1-e^{j2\pi\frac{k}{N}}z^{-1}}$ $k \in \{\pm1, \pm5, \pm7, \ldots\}$
The magnitude /phase adjustment γ	$\gamma = \begin{cases} \frac{6}{N[1-e^{j\frac{2\pi}{6}(-6k-2)}]} (k \in 6l+1,\ l = 0, \pm1, \ldots) \\ \frac{6}{N[1-e^{j\frac{2\pi}{6}(-6k+2)}]} (k \in 6l-1,\ l = 0, \pm1, \ldots) \end{cases}$

2) As shown in Section II, the comb filter determines the system dynamics; and in the GDFT, the comb filter can be configured in a compact form without unnecessary zeros, requiring less buffers and shorter delay time. Therefore, dynamics of the proposed GDFT can be improved.
3) Like the conventional DFT, the GDFT features selective harmonic extraction and excellent filtering abilities. Multiple resonators $H_r(z)$ and magnitude/phase adjustment factor γ can be paralleled to simultaneously extract multiple harmonics. And for the undesired harmonics, complete rejections are achieved due to the sets of zeros introduced by the comb filter.

To further show the features of the GDFT, an example is included. The comb filter is configured as (13) to extract the orders of $h_{1,2} = 6l \pm 1$ harmonics generated by the three-phase diode rectifiers [28]. Other Details are shown in Table I

$$H_c(z) = H^1_c(z)H^2_c(z) = \left(1 - z^{-\frac{N}{6}} e^{j\frac{2\pi}{6}}\right)\left(1 - z^{-\frac{N}{6}} e^{-j\frac{2\pi}{6}}\right). \quad (13)$$

And, the transfer function for extracting the fundamental positive sequence $\tilde{\tilde{x}}^{+1}_{\alpha\beta}$ can be derived as

$$H^{+1}_{\text{GDFT}}(z) = \gamma H_c(z) H^{+1}_r(z) = \frac{6}{N(1-e^{-j2\pi/3})}\left(1 - z^{-\frac{N}{6}} e^{j\frac{2\pi}{6}}\right)\left(1 - z^{-\frac{N}{6}} e^{-j\frac{2\pi}{6}}\right)\frac{1}{1-e^{j2\pi\frac{1}{N}}z^{-1}}. \quad (14)$$

Bode plot of the above transfer function is illustrated in Fig. 7. It can be clearly seen that zero attenuation and zero phase-shift at the selected frequency, i.e., the first-order, is achieved while at harmonic orders of -1, ±5, $\pm7, \ldots$, completely rejection, i.e., zero magnitude, can be seen. Moreover, the approximate $+20$ and -20 dB/dec roll-off of the magnitude envelope below and over the fundamental frequency helps to further attenuate the subharmonics.

Dynamic responses of the DFT and GDFT to a step sine input $\vec{x}_{\alpha\beta}(t) = e^{j\omega_0 t}$ are simulated in Simulink/MATLAB and compared in Fig. 8. It can be seen that the settling time for the GDFT is around 6.7 ms, which is only one-third of that of the conventional DFT.

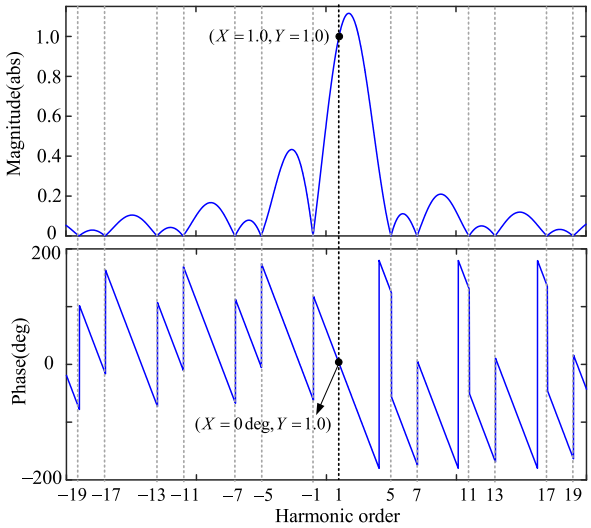

Fig. 7. Bode plot of the transfer function in (14) ($N = 198$).

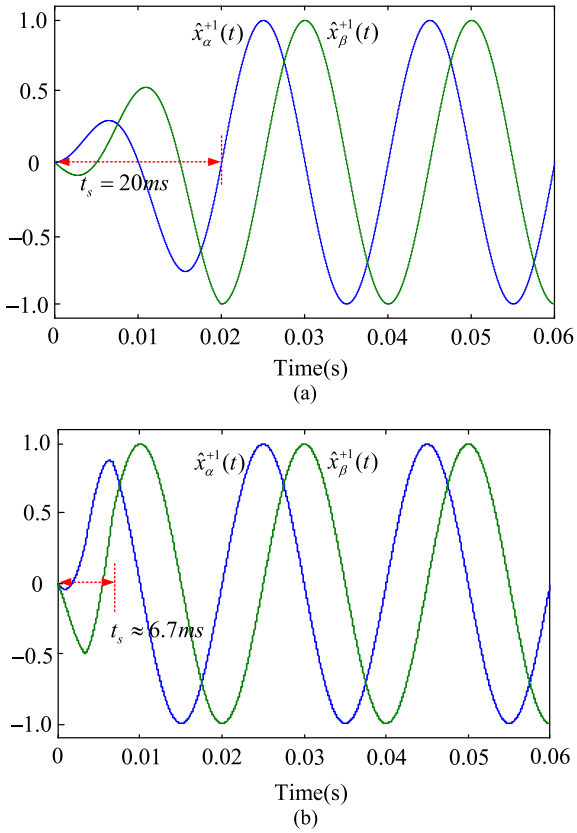

Fig. 8. Step responses of the DFT (a) and GDFT (b) filter for extracting the fundamental positive sequences, $N = 198$, $\omega_0 = 100\,\pi$.

It is worth noticing here that simulations of Fig. 8 are performed under the circumstances that the harmonic spectrum is balanced with orders of $h_{1,2} = 6l \pm 1$ (typically generated by the symmetrical three-phase diode rectifiers [28]). In case of unbalanced load harmonics, more comb filters should be cascaded, and the response tome may be up to one fundamental period.

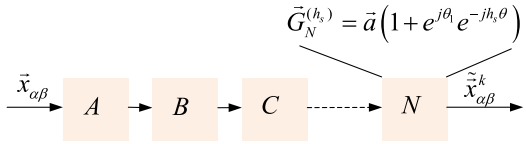

Fig. 9. Diagrams of the GDSC method [20], [21].

C. Comparisons With the Generalized Delayed Signal Cancellation (GDSC) Method

Selective harmonic extraction has been researched in many papers [7]–[25]. Among them, the GDSC [7], [20]–[21] technique as shown in Fig. 9, which features high flexibility, good accuracy, and good dynamics, is a typical and popular example. To provide more clear demonstrations of the method in the manuscript, detailed comparisons with the GDSC technique are presented.

1) The concepts or filtering mechanism of the two methods are different. The GDSC relies solely on cascaded delayed signal operators (see A–N in Fig. 9) for isolating the specific component and eliminating the rest. The GDFT, however, is based on pole-zero-cancellation mechanism, which is derived and extended from the conventional DFT via revelation and mathematical analysis. Although the DSC operators A–N in the GDSC and the comb filter $H_c(z)$ in GDFT are essentially the same, and they both achieve complete harmonic reject through introducing a set of zeros. However, DSC operators and $H_c(z)$ aim for different purposes and should be configured differently. The DSC operators are designed to pass through the selected frequency and eliminate the others. The $H_c(z)$ in the GDFT, however, shall reject at all the harmonic frequencies in the applied input signal, and then, the complex resonator $H_r^k(z)$ is included to produce a pole for pole-zero cancellation and to restore and extract the selected harmonic component.
2) Compared with the GDSC technique, which consisting of only comb filters, the proposed GDFT elaborately combines the comb filter with the complex resonator $H_r^k(z)$. And, it essentially behaves like a band-pass filter, which can help to further improve the filtering ability. To be more specific, take the typical harmonic scenario that contains $(+1, -1, -5, +7, +13, -17, +19, \ldots)$ in the distorted three-phase grid system as an example [26]. According to [7] and [20], the filter based on the GDSC method to extract the $+7$ component is

$$H_{\mathrm{GDSC}}^{+7}(z) = \frac{1}{2}\left(1 + z^{-\frac{N}{12}} e^{j\pi + j\frac{\pi}{6}}\right) \times \frac{1}{2}\left(1 + z^{-\frac{N}{24}} e^{j\pi - j\frac{5\pi}{12}}\right) \times \frac{1}{2}\left(1 + z^{-\frac{N}{48}} e^{j\pi - j\frac{17\pi}{24}}\right) \times \frac{1}{1 + e^{j\frac{2\pi}{3}}}\left(1 + z^{-\frac{N}{48}} e^{j\pi - j\frac{\pi}{24}}\right). \quad (15)$$

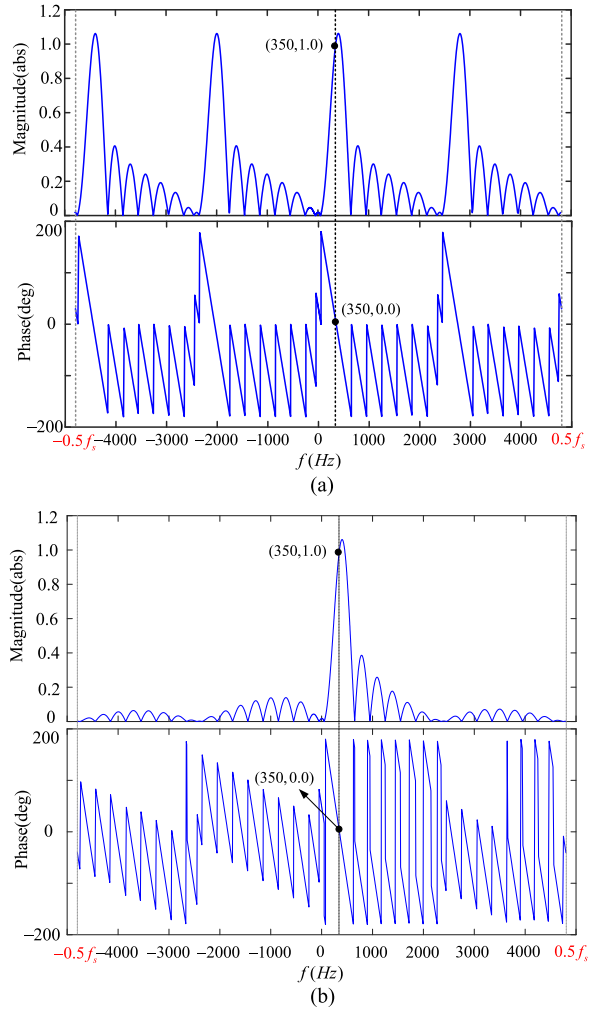

Fig. 10. Bode-plot comparisons of the (a) GDSC and (b) GDFT methods, $N = 192$, $\omega_0 = 100\,\pi$.

And, the GDFT method in the manuscript to detect the $+7$ component can be designed as

$$H^{+7}_{\mathrm{GDFT}}(z) = \gamma H_c(z) H_r^{+7}(z) = \frac{6}{N(1-e^{-j\frac{\pi}{3}})}\left(1 - z^{-\frac{N}{6}} e^{j\frac{2\pi}{6}}\right) \times \left(1 - z^{-\frac{N}{48}} e^{-j\frac{2\pi}{48}}\right) \frac{1}{1 - e^{j2\pi\frac{7}{N}} z^{-1}}. \quad (16)$$

These two filters in (1) and (2) have similar settling time with total delay of $1/12 + 1/24 + 1/48 + 1/48 \approx 0.17$ cycles and $1/6 + 1/48 \approx 0.19$ cycles, respectively. They can both completely reject harmonic components of $h = +1, -1, -5, +13, -17, +19, \ldots$, and accurately extract the $+7$ sequence as illustrated by the bode plots in Fig. 10.

Yet, from Fig. 10, it can be clearly seen that the proposed GDFT method features better band-pass filtering properties, approximate $+20$ and -20 dB/dec roll-off of the magnitude envelope below and over the $+7$th frequency, which helps to further attenuate the subharmonics and high frequency noise. As for the GDSC method, which consists of only comb filters,

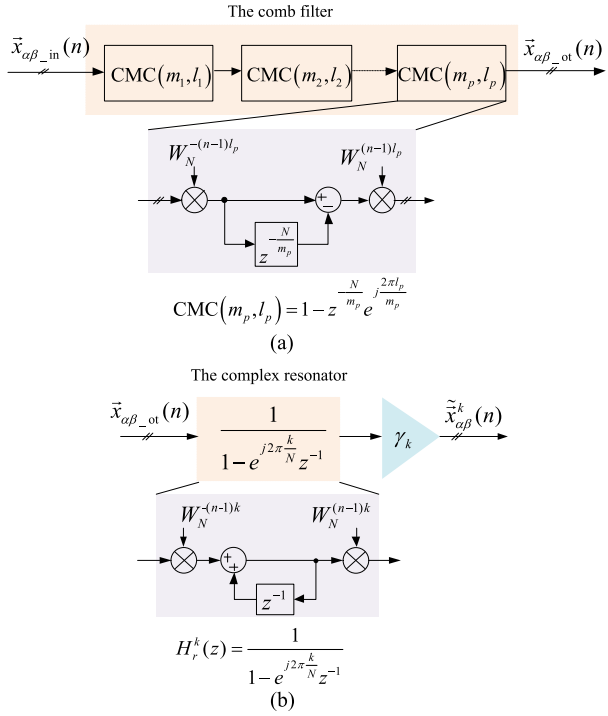

Fig. 11. Digital implementation of the proposed GDFT. (a) Implementation of the comb filter. (b) Implementation of the complex resonator.

the filtering performances are not satisfactory especially around frequencies of $h = 48n+7$. In fact, the GDSC provides zero attenuation at harmonic components of $h = 48n+7$ due to properties of periodical maxima (peaks) of the comb filters. It is worth noticing that the undesired peaks in Fig. 10(a) can be attenuated through cascading more DSC operators, yet at the cost of increased delay buffers, deteriorated dynamics and increased system complexity.

IV. Digital Implementations and Frequency Adaptability

A. Digital Implementation of the GDFT

The GDFT mainly consists of three parts, the comb filter $H_c(z)$, the complex resonator $H_r^k(z)$, and the adjustment factor γ. The can be easily realized through complex multiplication. The $H_c(z)$ and $H_r^{k_q}(z)$ can be implemented based on the "modulating properties" [24] as shown by Fig. 11, where $W_N^{-(n-1)l_p}$ is the complex twiddle factor and is equal to $\exp(-j(n-1)l_p 2\pi/N)$.Twiddle factors $W_N^{\pm(n-1)l_p}$ are time varying, depending on the sequence-index n. To avoid online calculation of trigonometric functions, sine/cosine tables can be prestored in the memory and then are retrieved for each new input $\vec{x}_{\alpha\beta}(n)$. Appendix B provides proof of the equivalence between the transfer function and its digital implementation. The comb filter consists of several subcomb-filters, CMC(m_1,l_1), CMC(m_2,l_2),. . . ,etc., [See (8)] connected in series, and can be realized through delay buffers, complex multiplication and subtraction. Output of the comb filter $\vec{x}_{\alpha\beta\_ot}(n)$ is shared by

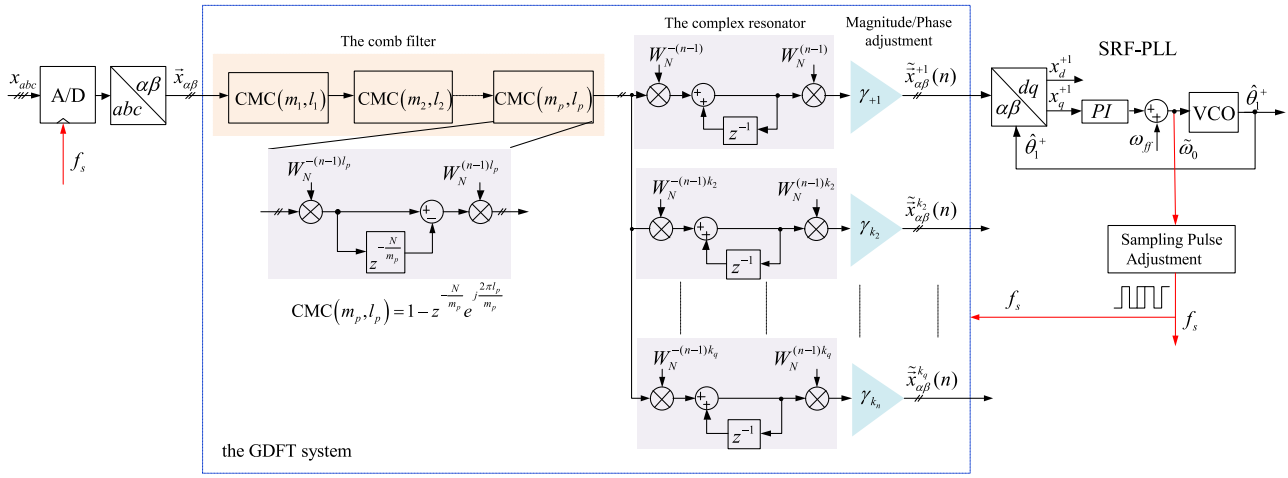

Fig. 12. Structure diagram of the proposed GDFT system with an SRF-PLL for frequency adaptive harmonic extraction.

the complex resonators. Each complex resonator corresponds to extracting one specific harmonic component.

B. Frequency Adaptability of the GDFT

In practical applications, grid or supply frequency disturbances are inevitable. If large frequency-disturbance is expected, it is necessary to include frequency-adaptive schemes into the GDFT to reduce the leakage effects and the detection errors.

Fig. 12 illustrates the control diagram with variable sampling frequency. The well-known synchronous reference frame phase-locked loop (SRF-PLL) [26] is incorporated to estimate the real-time grid frequency, which is then used to adjust the sampling rate of the entire detection system. Moreover, to avoid the influences of the harmonics on the PLL accuracy, the positive-sequence fundamental component $\vec{x}^{+1}_{\alpha\beta}(n)$ is first extracted by the GDFT before feeding to the SRF-PLL system. It is worth mentioning here that the proposed GDFT features short transients and therefore the bandwidth of the SRF-PLL can be set to a high value for fast dynamics [26]. Finally, with the estimated grid frequency $\tilde{\omega}_0$, sampling rate of the detection system is adjusted according to $f_s = N\tilde{\omega}_0/(2\pi)$, where N is the sample-points of the Fourier transform.

V. Simulative and Experimental Results

Simulative and experimental results are conducted to evaluate performances of the proposed harmonic detection methods. The control algorithms are implemented in a Field-Programmable Gate Array (FPGA, EP4CE40 from Altera, Inc.)–based control board. During the tests, the sample points N per fundamental period are fixed to be 768. Variable sampling frequency in Fig. 12 is achieved through dividing the main 50-MHz frequency. The input signals are sampled by the 14bit DAC (ADS7945) and are then fed to the FPGA control algorithms. The extracted results are output to the 16 bit DAC (DAC8501) and are displayed on the oscilloscope. In Section A, simulative tests are performed and the GDFT is designed for grid synchronization under adverse grid conditions. In Section B, the proposed technique is applied in the APF to compensate practical harmonics generated by the typical three-phase diode rectifiers that are widely used as the front-ends of industrial ac drives. Comparisons with the traditional DFT have also been conducted to show the advantages of the proposed method.

TABLE II
Parameters of the Distorted Voltages

Harmonic order h	Amplitude (p.u.)
Fundamental positive sequence $+1$	1.0
Fifth-harmonic negative sequence -5	0.034
Seventh-harmonic positive sequence $+7$	0.025
11th-harmonic negative sequence -11	0.092
13th-harmonic positive sequence $+13$	0.077
17th-harmonic negative sequence -17	0.009
19th-harmonic positive e sequence $+19$	0.009
23th-harmonic negative sequence -23	0.040
25th-harmonic positive sequence $+25$	0.035
31th-harmonic positive sequence $+31$	0.005

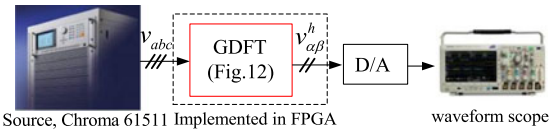

Fig. 13. Simulative diagram of the proposed GDFT system for extraction of harmonic voltages.

A. Extraction of Harmonic Voltages

In this case, the input three-phase voltage is generated by a programmable ac-power source (61511 from Chroma, Inc., Lititz, PA, USA) so as to incorporate harmonics and frequency variations. Specification of the distorted input voltages is listed in Table II. Control structure of the setup is illustrated in Fig. 13.

As shown in [26], the typical harmonic scenario in a distorted three-phase grid system is $h = +1, -1, -5, +7, +13, \ldots$. For this harmonic pattern, the comb filter $H_c(z)$ can be configured with two filter-cells connected in series ($m_1 = 6, l_1 = 1$; $m_2 = 24$, $l_2 = -1$) to effectively isolate harmonics with frequency orders of $h_1 = 6n+1$ ($+1, -5, +7, +13, -17, \ldots$) and $h_2 =$

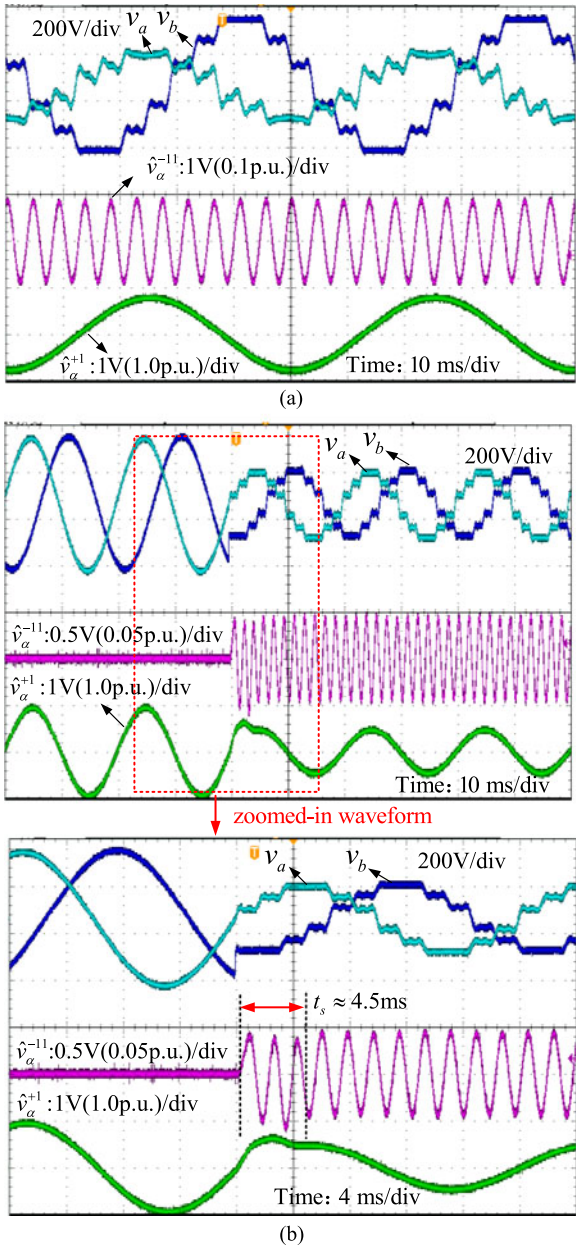

Fig. 14. Simulative results of the proposed GDFT under Test 1 (distorted voltages with constant frequency of 50Hz). (a) Steady steady results. (b) Dynamic results when the amplitude undergoes 0.5 p.u. drop and the harmonics are superposed.

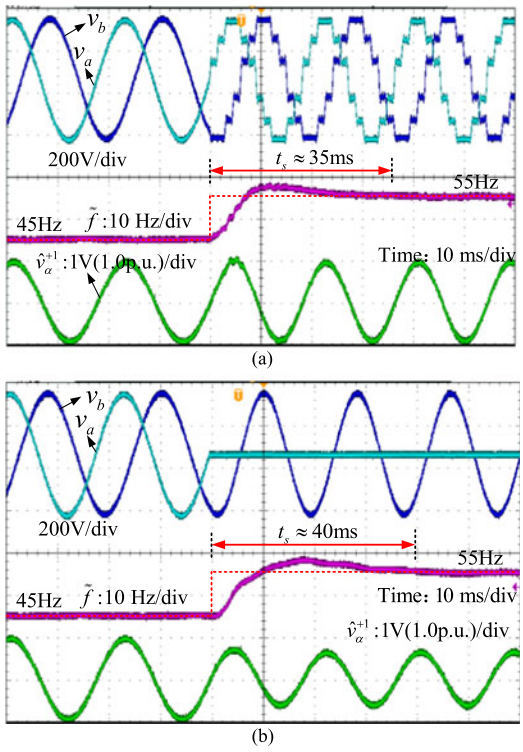

Fig. 15. Simulative results of the proposed GDFT when the grid frequency undergoes +10-Hz frequency jump. (a) Harmonics are superposed. (b) Amplitude of Phase A drops to zero.

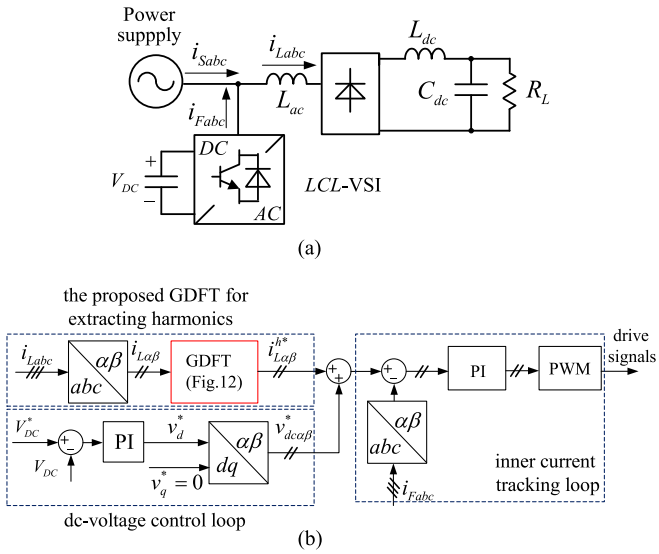

Fig. 16. Diagram of experimental setup and its control algorithm. (a) Structure of the experimental setup. (b) Control diagram of the active power filter.

$24n-1$ ($-1, +23, -25, \ldots$). And, the total delay time required is around 0.21 fundamental cycle (i.e., 1/6+1/24 = 5/24), which is much faster than that of the conventional DFT.

Test 1: Grid voltages with frequency of 50 Hz.

The proposed GDFT system is utilized to extract grid harmonic voltages with a constant grid frequency of 50 Hz, and the frequency adaptive scheme of SRF-PLL in Fig. 12 is disabled. Fig. 14 illustrates the simulative results under Test 1, where $v_{\rm a}$ and $v_{\rm b}$ refer to the input grid voltages; $\hat{v}_\alpha^{+1}$ and $\hat{v}_\alpha^{-11}$ are the detected stationary α-signals of the positive first and negative 11th sequences. It should be noted here that the fundamental positive sequence and the negative 11th sequences are extracted here as examples, and other harmonic voltages can be similarly detected through incorporating more complex resonators as shown in Fig. 6. It can be seen from Fig. 14(a) that the proposed GDFT system can accurately identify the harmonics voltages. Besides, it takes only around 4.5 ms for the proposed GDFT to reach into the steady state when the harmonics are superposed and the magnitude undergoes a 0.5 p.u. drop as shown in Fig. 14(b).

Test 2: Grid voltages with considerable frequency variations of step-change from 45 to 55 Hz.

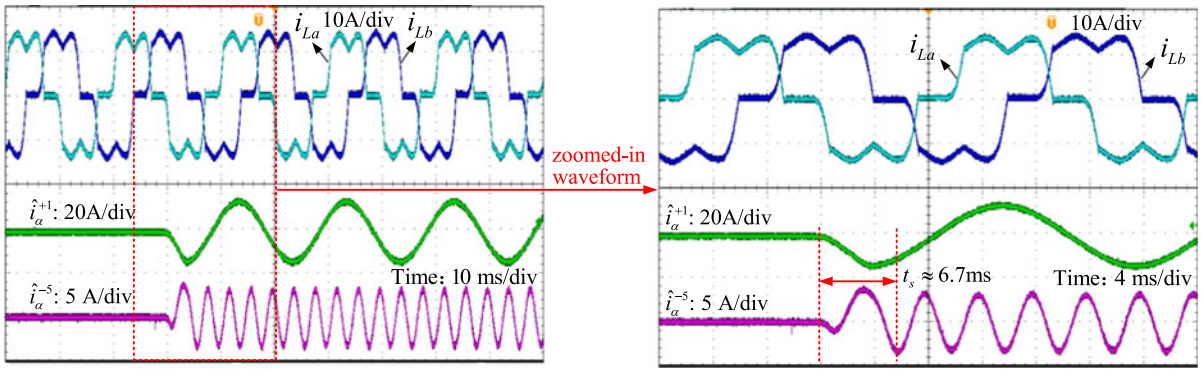

Fig. 17. Experimental results of the proposed GDFT for extracting harmonic currents.

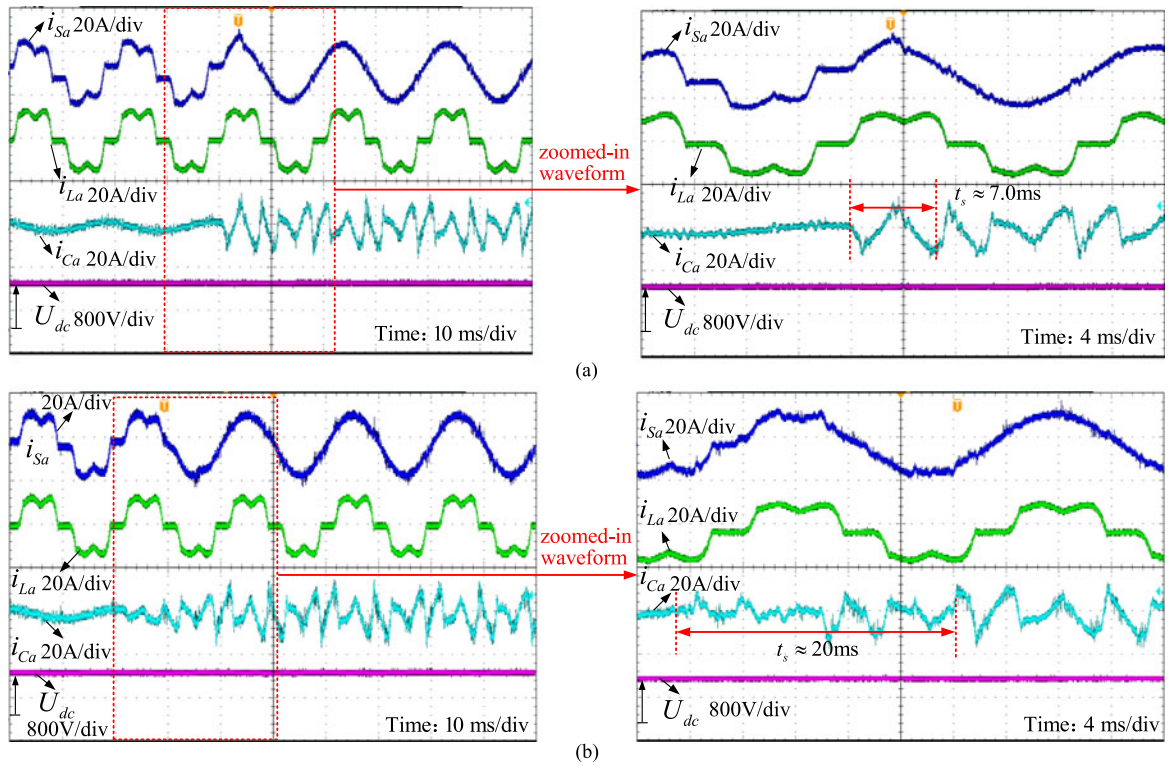

Fig. 18. Dynamic comparison results of the active power filter with the proposed GDFT and DFT. (a) APF with the GDFT. (b) APF with the conventional DFT.

Fig. 15 shows the simulative results when the grid frequency jumps from 45 to 55 Hz, where $v_{\rm a}$ and$v_{\rm b}$ refer to the input grid voltages; $\hat{v}_{\alpha}^{+1}$ is the detected stationary α-signals of the positive first sequences;$\hat{f}$ is the estimated grid frequency. In Fig. 15(a), the harmonic voltages are superposed at the same time, and in Fig. 15(b), amplitude of phase A drops to zero. It can be seen from Fig. 15, the proposed GDFT system requires around two fundamental cycles to reach the steady state, and after that, the harmonic voltages in the distorted grids can be accurately extracted.

B. Application in the APF and Comparisons With the DFT

The three-phase diode rectifiers are widely used as the front-ends of industrial ac drives. And the proposed GDFT system is applied to detect the generated harmonic currents. The rectifier is supplied by a 220 V-grid, and parameters for the nonlinear loads are $L_{\rm dc} = 10.7$ mH, $R_{\rm L} = 35\ \Omega$, $C_{\rm dc} = 4$ mF as shown by the diagram in Fig. 16(a). Further, a shunt APF is built to compensate the harmonic currents and improve the power quality. The control diagram of the APF is shown in Fig. 16(b). Harmonic currents in the distorted loads are extracted via the proposed GDFT as shown in Fig. 12 with the frequency adaptive loop disabled due to small frequency excursions in practical applications, and are then served as current references for the inner current loop. The inner current loop is controlled with a proportional-integral algorithm. The designed bandwidth is 4 kHz and 45° phase margin.

The harmonic currents generated by the three-phase diode rectifiers are typically nontriplen [28]. Therefore, in this application, the comb filter $H_{\rm c}(z)$ of the GDFT as in (14) is selected to filter and isolate the harmonics located at $h_{1,2} = 6n\pm1$ can be completely filtered and isolated. The total delay time is $1/3\approx0.33$ fundamental cycle, which is only one-third of the conventional DFT method.

The proposed GDFT system is applied to extract the typical harmonics generated by the three-phase diode rectifier. The experimental results is illustrated in Fig. 17, where i_{La} and i_{Lb} are the generated distorted currents; $\hat{i}_{\alpha}^{+1}$ and $\hat{i}_{\alpha}^{-5}$ are the detected stationary α-signals of the positive first and negative fifth current sequences. It can be clearly seen that the proposed technique can effectively isolate and extract the harmonics components, and the dynamic response time is only 6.7 ms, around 0.33 fundamental cycle.

A shunt APF is built to compensate the harmonic currents generated by the nonlinear three-phase diode rectifier and improve the power quality. The GDFT system extract the harmonics with orders of 5, 7, 11, 13, 17, 19, . . . , 35, 37, which are then summed together as the harmonic-current references for the inner current loop. Fig. 18 illustrates the experimental waveforms of the APF with the proposed GDFT and the conventional DFT, where i_{Sa}, i_{La}, and i_{Ca} are the source current, distorted load current, and compensated current in Phase A, respectively; U_{dc} is the dc voltage. Fig. 18(a) shows the dynamic waveforms when the APF utilizing the proposed GDFT is turned ON, and Fig. 18(b) illustrates the experimental results when the conventional DFT is used. THD of the source is reduced from 26.5% to 4.8% and 4.7% after applying the APF with the GDFT and DFT, respectively. And dynamic response time of the proposed GDFT is only 7.0 ms, around one-third of that of the conventional DFT.

VI. Conclusion

A fast and flexible selection harmonic detection method is proposed based on the deep revelation that the convention DFT can be viewed as a comb filter in series with complex resonators, and that it relies on the mechanism of pole-zero cancellation for harmonic isolation. The proposed method is referred to as the generalization DFT since it is an improved and generalized form of conventional DFT, where the comb filter and the adjustment factor are entirely reconfigured and reconstructed according to specific harmonic orders of the input signal for improving the dynamics and system flexibility. Tests results verify that the proposed GDFT can accurately detect the desired harmonic components from the input signal with fast dynamics, i.e., 0.3 fundamental cycle for practical APF applications, and around 2.0 cycle for 10-Hz grid-frequency step change.

Appendix

A. Derivation of the Transfer Function of the DFT

Equations (1) and (2) in Section II show the key equations of a DFT and an inverse DFT. Combing them yields

$$\tilde{\vec{x}}_{\alpha\beta}^{k}(n) = \frac{1}{N} e^{j2\pi\frac{kn}{N}} \sum_{i=n-N+1}^{n} \left[\vec{x}_{\alpha\beta}(i) e^{-j2\pi\frac{ki}{N}}\right]$$

$$= \frac{1}{N} e^{j2\pi\frac{kn}{N}} \sum_{J=0}^{N-1} \left[\vec{x}_{\alpha\beta}(n-J) e^{-j2\pi\frac{k}{N}(n-J)}\right]$$

$$= \frac{1}{N} \sum_{J=0}^{N-1} \left[\vec{x}_{\alpha\beta}(n-J) e^{j2\pi\frac{k}{N}J}\right]. \tag{A.1}$$

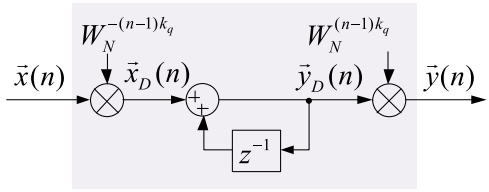

Fig. B.1. Implementation of the complex resonator.

Applying the z-transform to A.3, it is obtained

$$Z\left[\tilde{\vec{x}}_{\alpha\beta}^{k}(n)\right] = \frac{1}{N} Z\left\{\sum_{J=0}^{N-1}\left[\vec{x}_{\alpha\beta}(n-J) e^{j2\pi\frac{k}{N}J}\right]\right\}$$

$$= \frac{1}{N}\sum_{J=0}^{N-1}\left[Z\left[\vec{x}_{\alpha\beta}(n)\right] z^{-J} e^{j2\pi\frac{k}{N}J}\right]$$

$$= \frac{1}{N} Z\left[\vec{x}_{\alpha\beta}(n)\right] \frac{1-z^{-N}}{1-e^{j2\pi\frac{k}{N}} z^{-1}}. \tag{A.2}$$

Rearranging A.2 yields

$$G_{\mathrm{DFT}}^{k}(z) = \frac{Z\left[\tilde{\vec{x}}_{\alpha\beta}^{k}(n)\right]}{Z\left[\vec{x}_{\alpha\beta}(n)\right]} = \frac{1}{N}\frac{1-z^{-N}}{1-e^{j2\pi\frac{k}{N}} z^{-1}}. \tag{A.3}$$

B. Implementation of the Complex Resonator and the Comb Filter

This appendix is devoted to discussing realization of the complex resonator and the comb filter.

The diagram of implementing the complex resonator is shown in Fig. B.1. It will be proved that transfer function of diagram in Fig. B.1 is equivalent to

$$Z\left[\frac{\vec{y}(n)}{\vec{x}(n)}\right] = \frac{Y(z)}{X(z)} = \frac{1}{1-e^{j\frac{2\pi k_q}{N}} z^{-1}}. \tag{B.1}$$

From Fig. B.1, it can easily be obtained

$$\frac{Z\left[\vec{y}_D(n)\right]}{Z\left[\vec{x}_D(n)\right]} = \frac{1}{1-z^{-1}} \tag{B.2}$$

$$\begin{cases} \vec{x}_D(n) = \vec{x}(n) W_N^{-(n-1)k_q} \\ \vec{y}(n) = \vec{y}_D(n) W_N^{(n-1)k_q}. \end{cases} \tag{B.3}$$

Applying z-transform to (B.3), and recalling the following z-transform property, it is derived

$$\begin{cases} Z\left[\vec{x}_D(n)\right] = Z\left[\vec{x}(n) W_N^{-(n-1)k_q}\right] = X(W_N^{k_q} z) W_N^{k_q} \\ Z\left[\vec{y}(n)\right] = Z\left[\vec{y}_D(n) W_N^{(n-1)k_q}\right] = Y_D(W_N^{-k_q} z) W_N^{-k_q}. \end{cases} \tag{B.4}$$

Combing (B.2) and (B.3) yields

$$Z\left[\vec{y}(n)\right] = Y(z) = Y_D(W_N^{-k_q} z) W_N^{-k_q}$$

$$= \frac{X_D(W_N^{-k_q} z) W_N^{-k_q}}{1 - W_N^{k_q} z^{-1}} = \frac{X(z)}{1 - W_N^{k_q} z^{-1}}. \tag{B.5}$$

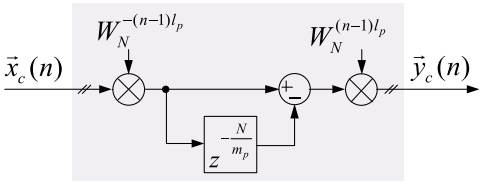

Fig. B.2. Implementation of the comb filter.

Therefore

$$\frac{Y(z)}{X(z)} = \frac{1}{1 - e^{j\frac{2\pi k_q}{N}} z^{-1}}. \tag{B.6}$$

Following the same procedure as above, the transfer function of the diagram in Fig. B.2, which is used for realizing the comb filter, can be derived as

$$Z\left[\frac{\vec{y}_c(n)}{\vec{x}_c(n)}\right] = 1 - z^{-\frac{N}{m_p}} e^{j\frac{2\pi l_p}{m_p}}. \tag{B.7}$$

REFERENCES

[1] L. Asiminoaei, F. Blaabjerg, and S. Hansen, "Detection is key—Harmonic detection methods for active power filter applications," *IEEE Ind. Appl. Mag.*, vol. 13, no. 4, pp. 22–33, Jul./Aug. 2007.

[2] J. Ortega, M. Esteve, M. Payan, A. Exposito, and L. Franquelo, "Reference current computation methods for active power filters: Accuracy assessment in the frequency domain," *IEEE Trans. Power Electron.*, vol. 20, no. 2, pp. 446–456, Mar. 2005.

[3] Y. W. Li and J. He, "Distribution system harmonic compensation methods: An overview of DG-Interfacing inverters," *IEEE Ind. Electron. Mag.*, vol. 8, no. 12, pp. 18–31, Dec. 2014.

[4] Z. Zeng, H. Yang, S. Tang, and R. Zhao, "Objective-oriented power quality compensation of multifunctional grid-tied inverters and its application in microgrids," *IEEE Trans. Power Electron.*, vol. 30, no. 3, pp. 1255–1265, Mar. 2015.

[5] F. D. Freijedo, J. Doval-Gandoy, Ó. LÓpez, and E. Acha, "A generic open-loop algorithm for three-phase grid voltage/current synchronization with particular reference to phase, frequency, and amplitude estimation," *IEEE Trans. Power Electron.*, vol. 24, no. 1, pp. 94–107, Mar. 2009.

[6] H. Liu, Y. Xing, and H. Hu, "Enhanced frequency-locked loop with a comb filter under adverse grid conditions," *IEEE Trans. Power Electron.*, vol. 31, no. 12, pp. 8046–8051, Dec. 2016.

[7] Y. F. Wang and Y. W. Li, "Three-Phase cascaded delayed signal cancellation PLL for fast selective harmonic detection," *IEEE Trans. Ind. Electron.*, vol. 60, no. 4, pp. 1452–1463, Apr. 2013.

[8] X. Yuan, W. Merk, H. Stemmler, and J. Allmeling, "Stationary-frame generalized integrators for current control of active power filters with zero steady-state error for current harmonics of concern under unbalanced and distorted operating conditions," *IEEE Trans. Ind. Appl.*, vol. 38, no. 2, pp. 523–532, Mar./Apr. 2002.

[9] P. Cheng, C. Chen, T. Lee, and S. Kuo, "A cooperative imbalance compensation method for distributed-generation interface converters," *IEEE Trans. Ind. Appl.*, vol. 45, pp. 805–815, Mar./Apr. 2009.

[10] P. Xiao, K. A. Corzine, and G. K. Venayagamoorthy, "Multiple reference frame-based control of three-phase PWM boost rectifiers under unbalanced and distorted input conditions," *IEEE Trans. Power Electron.*, vol. 23, no. 4, pp. 2006–2017, Jul. 2008.

[11] L. Hadjidemetriou, E. Kyriakides, and F. Blaabjerg, "A robust synchronization to enhance the power quality of renewable energy systems," *IEEE Trans. Ind. Electron.*, vol. 62, no. 8, pp. 4858–4868, Aug. 2015.

[12] D. Yazdani, A. Bakhshai, and P. K. Jain, "A three-phase adaptive notch filter-based approach to harmonic/reactive current extraction and harmonic decomposition," *IEEE Trans. Power Electron.*, vol. 25, no. 4, pp. 914–923, Apr. 2010.

[13] P. Rodriguez, A. Luna, I. Candela, R. Mujal, R. Teodorescu, and F. Blaabjerg, "Multiresonant frequency-locked loop for grid synchronization of power converters under distorted grid conditions," *IEEE Trans. Ind. Electron.*, vol. 58, no. 1, pp. 127–138, Jan. 2011.

[14] Y. F. Wang and Y. W. Li, "A grid fundamental and harmonic component detection method for single-phase systems," *IEEE Trans. Power Electron.*, vol. 28, no. 5, pp. 2204–2213, May 2013.

[15] H. Akagi, Y. Kanazawa, and A. Nabae, "Instantaneous reactive power compensators comprising switching devices without energy storage components," *IEEE Trans. Ind. Appl.*, vol. 20, no. 3, pp. 625–630, May 1984.

[16] A. Bagheri, M. Mardaneh, A. Rajaei, and A. Rahideh, "Detection of grid voltage fundamental and harmonic components using kalman filter and generalized averaging method," *IEEE Trans. Power Electron.*, vol. 31, no. 2, pp. 1064–1073, Feb. 2016.

[17] G. De Donato, G. Scelba, G. Borocci, F. Giulii Capponi, and G. Scarcella, "Fault-decoupled instantaneous frequency and phase angle estimation for three-phase grid-connected inverters," *IEEE Trans. Power Electron.*, vol. 31, no. 4, pp. 2880–2889, Apr. 2016.

[18] S. A. Gonzalez, R. Garcia-Retegui, and M. Benedetti, "Harmonic computation technique suitable for active power filters," *IEEE Trans. Ind. Electron.*, vol. 54, no. 5, pp. 2791–2796, Oct. 2007.

[19] E. Lavopa, P. Zanchetta, M. Sumner, and F. Cupertino, "Real-time estimation of fundamental frequency and harmonics for active shunt power filters in aircraft electrical systems," *IEEE Trans. Ind. Electron.*, vol. 56, no. 8, pp. 2875–2884, Jan. 2009.

[20] F. A. S. Neves, H. E. P. de Souza, F. Bradaschia, M. C. Cavalcanti, M. Rizo, and F. J. Rodriguez, "A space-vector discrete Fourier transform for unbalanced and distorted three-phase signals," *IEEE Trans. Ind. Electron.*, vol. 57, no. 8, pp. 2858–2867, Aug. 2010.

[21] F. A. S. Neves, H. E. P. de Souza, F. Bradaschia, and E. J. Bueno, "Digital filters for fast harmonic sequence component separation of unbalanced and distorted three-phase signals," *IEEE Trans. Ind. Electron.*, vol. 59, no. 10, pp. 3847–3859, Oct. 2012.

[22] E. Jacobsen and R. Lyons, "The sliding DFT," *IEEE Signal Process. Mag.*, vol. 20, no. 2, pp. 74–80, Mar. 2003.

[23] E. Jacobsen and R. Lyons, "An update to sliding DFT," *IEEE Signal Process. Mag.*, vol. 21, no. 1, pp. 110–111, Jan. 2004.

[24] K. Duda, "Accurate, guaranteed stable, sliding discrete Fourier transform [DSP tips & tricks]," *IEEE Signal Process. Mag.*, vol. 27, no. 6, pp. 124–127, Nov. 2010.

[25] F. A. S. Neves, M. A. C. Arcanjo, G. M. S. Azevedo, H. E. P. de Souza, and L. T. L. Viltre, "The SVFT-based control," *IEEE Trans. Ind. Electron.*, vol. 61, no. 8, pp. 4152–4160, Aug. 2014.

[26] S. Golestan, M. Monfared, and F. D. Freijedo, "Design-oriented study of advanced synchronous reference frame phase-locked loops," *IEEE Trans. Power Electron.*, vol. 28, no. 2, pp. 765–778, Feb. 2013.

[27] D. S. Carter,, "L′Hospital′s rule for complex-valued functions," *Amer. Math. Monthly*, vol. 65, no. 4, pp. 68–69, Apr. 1958.

[28] C. Lascu, L. Asiminoaei, I. Boldea, and F. Blaabjerg, "High performance current controller for selective harmonic compensation in active power filters," *IEEE Trans. Power Electron.*, vol. 22, no. 5, pp. 1826–1835, Sep. 2007.

Huawu Liu (S'14) received the B.S. degree in electrical engineering from Nanjing University of Aeronautics and Astronautics (NUAA), Nanjing, China, in 2008. He is currently working toward the Ph.D. degree in electrical engineering in NUAA.

His current research interests include topology and control of high-step-up dc-dc converters, and active power filters.

Haibing Hu (M'09) received the B.S. degree from Hunan University of Technology, Zhuzhou, China, in 1995, the M.S and Ph.D. degrees from Zhejiang University, Hangzhou, China, in 2003 and 2007, respectively, all in electrical engineering.

Since 2007, he has been with the Faculty of Electrical Engineering, Nanjing University of Aeronautics and Astronautics (NUAA), Nanjing, China, and is currently a Professor with the College of Automation Engineering, NUAA. His research interests include digital control in power electronics, multilevel inverter, digital control system integration for power electronics, and applying power electronics to distributed energy systems and power quality.

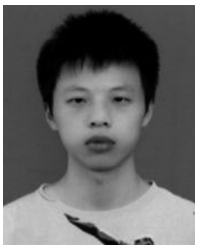

Hao Chen received the B.S. degree in electrical engineering from Nanjing University of Aeronautics and Astronautics (NUAA), Nanjing, China, in 2016. He is currently working toward the M.S degree in electrical engineering from NUAA.

His current research interests include topology and digital control in power electronics, and active power filters.

Li Zhang (S'11–M'13) received the B.E. and Ph.D. degrees in electrical engineering from Nanjing University of Aeronautics and Astronautics (NUAA), Nanjing, China, in 2007, and 2012, respectively.

From October 2012 to September 2014, he was a Postdoctoral Research Fellow with the Department of Electrical Engineering, Tsinghua University, Beijing, China. In 2014, he joined the Faculty of Electrical Engineering, Hohai University, Nanjing, China, and is currently an Associate Professor. His main research interests include topology, control of dc–ac converter, and distributed generation technology.

Dr. Zhang received the IEEE TRANSACTIONS ON POWER ELECTRONICS' Outstanding Reviewer Award in 2014

Yan Xing (M'03) received the B.S. and M.S. degrees in automation and electrical engineering from Tsinghua University, Beijing, China, in 1985 and 1988, respectively, and the Ph.D. degree in electrical engineering from Nanjing University of Aeronautics and Astronautics (NUAA), Nanjing, China, in 2000.

Since 1988, she has been with the Faculty of Electrical Engineering, NUAA, and is currently a Professor with the College of Automation Engineering, NUAA. She has authored more than 200 technical papers published in journals and conference proceedings and has also published three books. Her research interests include topology and control for dc–dc and dc–ac converters.